Rectifier Load Analysis for Electric Vehicle Wireless Charging System

Yanjie Guo, Lifang Wang, *Member, IEEE*, Yuwang Zhang,
Shufan Li, and Chenglin Liao, *Member, IEEE*

***Abstract*—This paper presents the analysis of rectifier load used for electric vehicle (EV) wireless charging system, as well as its applications on compensation network design and system load estimation. Firstly, a rectifier load model is established to get its equivalent input impedance, which contains both resistance and inductance components, and can be independently calculated through the parameters of the rectifier circuit. Then, a compensation network design method is proposed, based on the rectifier load analysis. Furthermore, a secondary side load estimation method and a primary side load estimation method are put forward, which adopt only measured voltages and consider the influence of the rectifier load. Finally, an EV wireless charging prototype is developed, and experimental results have proved that the rectifier equivalent load can be correctly calculated on conditions of different system load resistances, rectifier input inductances, DC voltages, and mutual-inductances. The experiments also show that rectifier load equivalent inductance will impact system performances, and the proposed methods have good accuracy and robustness in the cases of system parameter variations.**

***Index Terms*—Wireless charging system, rectifier load, compensation network design, load estimation.**

NOMENCLATURE

U_d	DC voltage source.
G_1 - G_4	Primary side MOSFETs.
D_1 - D_4	Secondary side diodes.
L_1 R_1 Z_1	Self-inductance, resistance, and self-impedance of the transmit coil.
L_2 R_2 Z_2	Self-inductance, resistance, and self-impedance of the receive coil.
M Z_m	Mutual-inductance and mutual-impedance between the two coupling coils.
L_p R_{Lp} Z_p	Inductance, resistance, and impedance of the primary side compensation inductor.
L_s R_{Ls} Z_s	Inductance, resistance, and impedance of the secondary side compensation inductor.
C_{1s} R_{1s} Z_{1s}	Capacitance, resistance, and impedance of the primary side series compensation capacitor.
C_{1p} R_{1p} Z_{1p}	Capacitance, resistance, and impedance of the primary side parallel compensation capacitor.
C_{2s} R_{2s} Z_{2s}	Capacitance, resistance, and impedance of the secondary side series compensation capacitor.
C_{2p} R_{2p} Z_{2p}	Capacitance, resistance, and impedance of the secondary side parallel compensation capacitor.
C_{in}	System input filter capacitor.
C_o R_{Co}	Capacitance and resistance of the system output filter capacitor.
R_L	System equivalent load resistance.
ω	System angle frequency.
u_s V_s	Voltage source of the rectifier circuit and its amplitude.
u_{rec} i_{rec}	Rectifier input voltage and current.
θ_b θ_f	Start and end phase angles of u_{rec} and i_{rec}.
u_{dio} V_{dio}	Diode forward voltage drop and its value.
R_{dio}	Diode conduction resistance.
u_d V_d	Load voltage and its approximate DC value.
i_d I_d	Load current and its approximate DC value.
$\Phi(t)$	Characteristic matrix of the rectifier circuit.
U_{rec_fd} φ_{urec_fd}	Fundamental amplitude and phase angle of u_{rec}.
I_{rec_fd} φ_{irec_fd}	Fundamental amplitude and phase angle of i_{rec}.
R_e L_e	Series equivalent resistance and inductance of the rectifier load.
Z_{s1}	Impedance after the secondary side series compensation capacitor C_{2s}.
Z_{p1}	Impedance after the primary side compensation inductor L_p.
η_c	Efficiency from inverter output to rectifier load equivalent impedance R_e and L_e.
R_{opt}	Optimal resistance in the secondary side.
R_{es}	Equivalent resistance of the secondary side, when C_{2s} and C_{2p} are well designed.
u_{inv} U_{inv}	Inverter output voltage and its RMS value.
P_{or} η_r	Rated system output power and efficiency.
L_{soft}	Inductance needed for inverter soft switching.
R_{L_Sesti}	Estimated load resistance adopting the proposed

Manuscript received May 11, 2017; revised August 29, 2017 and November 30, 2017; accepted December 21, 2017. This work was supported by National Natural Science Foundation of China (51507168), International Science & Technology Cooperation Program of China (2016YFE0102200), and the State Key Laboratory of Automotive Safety and Energy of China (KF16012).

Y. J. Guo, L. F. Wang, and C. L. Liao are with the Key Laboratory of Power Electronics and Electric Drives, Institute of Electrical Engineering, Chinese Academy of Sciences, Beijing 100190, China, and also with the Beijing Co-Innovation Center for Electric Vehicles, Beijing 100081, China (e-mail: yjguo@mail.iee.ac.cn; wlf@mail.iee.ac.cn; liaocl@mail.iee.ac.cn).

Y. W. Zhang, and S. F. Li are with the Key Laboratory of Power Electronics and Electric Drives, Institute of Electrical Engineering, Chinese Academy of Sciences, Beijing 100190, China, and also with the University of Chinese Academy of Sciences, Beijing 100190, China (e-mail: zhangyuwang@mail.iee.ac.cn; lishufan@mail.iee.ac.cn).

	secondary side load estimation method.
R_{L_Pesti}	Estimated load resistance adopting the proposed primary side load estimation method.
t_{ucs}	Positive zero crossing time of the voltage before rectifier input inductor.
t_{urs}	Positive zero crossing time of the rectifier input voltage following t_{ucs}.
G_p	Fundamental voltage transfer function between the inverter output voltage and the voltage after inverter output inductor.
G_s	Fundamental voltage transfer function between the voltage before rectifier input inductor and the rectifier input voltage.
Z_{11} Z_{12} Z_{21} Z_{22}	Impedance parameters of the equivalent two-port network of the coupling coils and compensation capacitors.
n_1 n_2 d_1 d_2	Impedance coefficients in the relationship equation between G_p and G_s.
Amp Php	Amplitude and phase angle of G_p.
θ_n θ_d	Phase angles of the numerator and denominator of G_s.
*amn*1 *phn*1	Amplitude and phase angle of n_1.
*amd*1 *phd*1	Amplitude and phase angle of d_1.
*ren*2 *imn*2	Real and imaginary parts of n_2.
*red*2 *imd*2	Real and imaginary parts of d_2.
T_j	Diode junction temperature in degrees Celsius.

I. Introduction

ELECTRIC vehicle (EV) wireless charging system (WCS) has the advantages of convenience, space-saving, etc. So, it has attracted much attention. In recent years, working principle, operation characteristics, system design, and control method of both stationary and dynamic wireless EV charging systems have been studied and applied to some demonstrations [1,2].

In applications of EV wireless charging, rectifier and output filter capacitor are needed to convert the high frequency AC to DC, in order to charge the power battery. Rectifier and the circuit after it are usually equivalent to a pure resistance load to design the system or control strategy [3,4]. A conventional way is using the coefficient $8/\pi^2$ to make an equivalent relationship between the rectifier input impedance and the system load resistance [5,6]. However, stray parameters and non-ideal behaviors of the devices will become obvious at the high frequency range [7]. Also, rectifier input impedance can be affected by the input inductance and other parameters. So, it will bring some deviations, if only considering WCS rectifier input impedance as a pure resistance.

Actually, rectifier input impedance of EV wireless charging system contains both resistance part and inductance part [7-9]. It can be expressed as a series of an equivalent resistance and an equivalent inductance [8,9]. Although there has not been an effective method to get the equivalent load impedance of WCS rectifier, some existing researches could be helpful. Based on the on and off states [10], the rectifier and its related inductance and capacitance circuits can be described by the state space model [11], considering the stray resistances and diode forward voltage drop [12]. Then, the expressions of the related voltages and currents have been obtained in the time domain, frequency domain, or complex frequency domain [13,14], which can be used for the analysis of WCS rectifier equivalent load impedance. Besides, non-linear switching functions and circuit simulations could also be adopted to study this issue [15].

The non-linear process of rectifier load will bring some difficulties to system compensation network design. As we know, compensation networks are very important to system performances [16], and can be designed to achieve maximum efficiency, maximum power, or conjugate matching [17,18]. In most cases, a pure resistance is used to express the rectifier load [19-21]. But the operation modes of WCS rectifier load will affect the working states of compensation network [22]. So, actual equivalent input impedance of WCS rectifier load should be considered, while designing the compensation networks.

Load estimation of WCS has faced the same problem. Effects of the rectifier load could complicate the equations used for load estimation [23], and lead to the increasing of calculation and control complexity. Hence, a pure resistance load is approximately used for most of the load estimation, detection, or optimal load tracking [24-26]. Another situation is that the voltages and currents are usually both measured for load estimation, in order to calculate the impedances in the primary side [24,27]. Since the voltage and current sensors or probes have different phase delays at the high frequency range, some deviations may be introduced into the estimation process. Also, the robustness of the estimation method is very important. It can be analyzed through parameter derivation, root locus, Nyquist curve, Bode graph, or directly calculating the results on conditions of parameter variations [28-30].

Based on the previous researches, an effective method to quantitatively analyze the equivalent load of WCS rectifier is put forward in the paper firstly. The equivalent load can be independently calculated through the parameters of the rectifier circuit, and the results are basically not affected by other WCS parts. Secondly, a compensation network design method is proposed considering the equivalent impedance of the rectifier load, especially the equivalent inductance. This method will further decouple the primary and secondary side design, to achieve four system performance indicators at the same time. Thirdly, the effects of the rectifier non-linear process are taken into count to estimate the system load resistance. The proposed primary side load estimation method only adopts high frequency voltages, does not need to measure the currents, and can avoid the phase delay deviations. Also, it does not require wireless communication between the primary and secondary sides. This paper is organized as follows. Section II establishes the rectifier load model and shows the equivalent input impedance calculations. Section III presents the compensation network design method. Section IV proposed the load estimation methods based on primary and secondary side voltage measurements. Section V gives the experimental verifications and discussions.

II. Rectifier Load Analysis And Calculation

Full-bridge diode rectifier is the most commonly used topology in EV wireless charging system. Also, dual-side *LCC*

This article has been accepted for publication in a future issue of this journal, but has not been fully edited. Content may change prior to final publication. Citation information: DOI 10.1109/TIE.2018.2793260, IEEE Transactions on Industrial Electronics

compensation networks can provide several appropriate design degrees of freedom to achieve several system performance indicators at the same time. Moreover, it can be designed to make the system resonant frequency independent of the load condition [16,22]. So we discuss the rectifier load on the basis of this kind of topology.

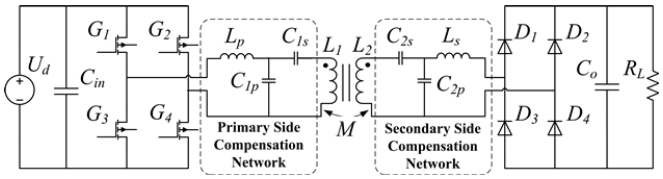

Fig. 1. EV wireless charging system with full-bridge diode rectifier and dual-side *LCC* compensation networks.

Fig.1 shows the EV wireless charging system with full-bridge diode rectifier and dual-side *LCC* compensation networks; where, U_d is DC voltage source; the high frequency inverter is composed of G_1-G_4, and the full-bridge rectifier is composed of D_1-D_4; the primary side compensation network consists of L_p, C_{1s}, and C_{1p}; the secondary side compensation network consists of L_s, C_{2s}, and C_{2p}; L_1 and L_2 are self-inductances of the transmit coil and receive coil; M is mutual-inductance between them; C_{in} and C_o are system input and output filter capacitors; R_L is system load resistor. It should be noticed that the WCS load is an EV power battery in the practical case, which behaves as a voltage source series with its parasitic resistance. But the power battery could be equivalent to a load resistance R_L [1,19]; the value of this equivalent resistance can be calculated by the voltage on the power battery divided by the current flowing through it. Moreover, the full-bridge rectifier, its input inductor, output filter capacitor, and the load resistor are together defined as the rectifier circuit. Although the following analysis is conducted based on the specific system, it can be extended to applications on other rectifier and compensation network topologies.

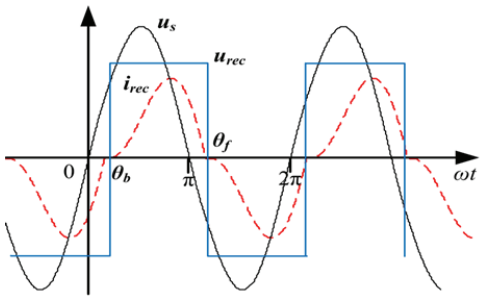

Fig. 2. Schematic waveforms of the source voltage, rectifier input voltage and current.

In order to calculate rectifier equivalent input impedance, we firstly need to analyze the voltages and currents of rectifier circuit, which are shown in Fig.2; where, u_s is the voltage on C_{2p}, which is a sine wave [22], and can be treated as the voltage source of the rectifier circuit; u_{rec} and i_{rec} are rectifier input voltage and current; the start time of u_s positive half-cycle is selected as the coordinate zero of x-axis. θ_b and θ_f are start and end phase angles of u_{rec} and i_{rec}. So, $\theta_f=\theta_b+\pi$. Also, the rectifier input inductance L_s should be big enough to keep the rectifier working in the continuous conduction mode (CCM), in order to avoid too large current peaks in the diodes. Hence, only CCM states are shown in Fig.2, and discussed in this paper. Besides, the steady state waveforms of u_{rec} and i_{rec} are presented in Fig.2, when only a few fluctuations exist on the voltage of the output capacitor C_o and the voltage drop on R_{Co} is very small. So, u_{rec} can be approximately described as a square wave.

Fig.2 suggests that the waveform of rectifier input current i_{rec} has some distortion, because of the effect of the rectifier input inductance. This makes the fundamental wave of i_{rec} lags behind the one of u_{rec}. So, the rectifier input impedance does not just include resistance component, but also contains a certain inductance component. Moreover, Fig.2 shows that the positive and negative half-cycles are symmetric for all the voltage and current waveforms. Hence, we just need to consider the positive half-cycle, and the negative half-cycle can be obtained from the symmetry. Fig.3 shows the equivalent circuit of the rectifier circuit in the positive half cycle, considering the stray parameters and the diode forward voltage drop; where, u_{dio} represents the diode forward voltage drop; R_{dio} is diode conduction resistance; R_{Ls} and R_{Co} are stray resistances of L_s and C_o, respectively; u_d and i_d are load voltage and current.

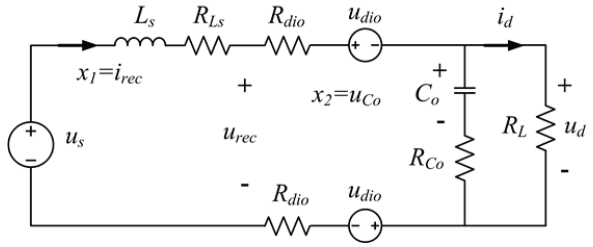

Fig. 3. Equivalent circuit of the rectifier circuit in the positive half cycle.

Based on the equivalent circuit, i_{rec} is defined as state variable x_1, and the voltage on C_o is defined as state variable x_2. u_s and u_{dio} are treated as the input variables, and u_d is treated as the output variable. So, state space equation of the rectifier circuit in the positive half cycle is given by (1a).

$$\begin{bmatrix} x_1' \\ x_2' \end{bmatrix} = \mathbf{A}\begin{bmatrix} x_1 \\ x_2 \end{bmatrix} + \mathbf{B}\begin{bmatrix} u_s \\ u_{dio} \end{bmatrix}, \quad y = \mathbf{C}\begin{bmatrix} x_1 \\ x_2 \end{bmatrix}. \tag{1a}$$

Where, impedance matrixes **A**, **B**, and **C** are given by (1b).

$$\mathbf{A} = \begin{bmatrix} -\frac{1}{L_s}\left(R_{Ls} + 2R_{dio} + \frac{R_L R_{Co}}{R_L + R_{Co}}\right) & -\frac{1}{L_s}\left(1 - \frac{R_{Co}}{R_L + R_{Co}}\right) \\ \frac{R_L}{C_o(R_L + R_{Co})} & -\frac{1}{C_o(R_L + R_{Co})} \end{bmatrix}, \tag{1b}$$

$$\mathbf{B} = \begin{bmatrix} 1/L_s & -2/L_s \\ 0 & 0 \end{bmatrix}, \quad \mathbf{C} = \begin{bmatrix} \frac{R_L R_{Co}}{R_L + R_{Co}} & 1 - \frac{R_{Co}}{R_L + R_{Co}} \end{bmatrix}.$$

Then, the input variables and the initial values of the state variables are given by (2), according to the schematic waveforms in Fig.2; where, ω is system angle frequency; the diode forward voltage drop is treated as a constant value V_{dio}. Since only a few fluctuations exist on the voltage of C_o and the voltage drop on R_{Co} is very small, their influences can be ignored, and the initial value of x_2 can be approximately equivalent to a DC voltage variable V_d. Also, amplitude of u_s is defined as V_s, and it will be affected by WCS parameters, such

as source voltage, mutual-inductance, etc. But the amplitudes of u_{rec} and i_{rec} are proportional to V_s. So, V_s can be treated as a known variable.

$$u_{s+} = V_s \sin(\omega t + \theta_b),\quad u_{dio} = V_{dio},\quad \boldsymbol{x}_+(0) = \left[0, V_d\right]^T. \quad (2)$$

Furthermore, V_d and θ_b should be calculated to solve the state space equation. On the WCS normal working conditions, the value of V_{dio} and the voltage drops on R_{dio} and R_{Ls} are much smaller than the ones of V_s and V_d. So, the voltage on L_s is approximately equivalent to $V_s \sin\theta$ - V_d, and the expression of i_{rec} can be given by (3), according to the relationship between the voltage on an inductor and the current flowing through it.

$$i_{rec} = \frac{1}{\omega L_s}\int_{\theta_b}^{\theta}(V_s \sin\theta - V_d)d\theta. \quad (3)$$

As shown in Fig.2, i_{rec}=0, when θ=θ_f=θ_b+π. So, one relationship between V_d and θ_b can be got and given by (4).

$$V_d = (2V_s \cos\theta_b)/\pi. \quad (4)$$

Also, the DC load current I_d can be calculated by (5), which is the average value of i_d in the positive half cycle.

$$\begin{aligned} I_d &= \frac{1}{\pi\omega L_s}\int_{\theta_b}^{\theta_b+\pi}\int_{\theta_b}^{\theta}(V_s \sin\theta - V_d)d\theta \\ &= (V_s(2\sin\theta_b + \pi\cos\theta_b) - \pi^2 V_d/2)/\pi\omega L_s. \end{aligned} \quad (5)$$

Because I_d=V_d/R_L, another relationship between V_d and θ_b can be got and given by (6).

$$V_d = V_s(2\sin\theta_b + \pi\cos\theta_b)/(\pi(\omega L_s/R_L + \pi/2)). \quad (6)$$

Based on the two relationships between V_d and θ_b, they can be obtained from (4) and (6). The expression of θ_b is given by (7), and the expression of V_d can also be got according to their relationships. Equation (7) indicates that the phase difference between u_s and u_{rec} (or i_{rec}) is mainly decided by L_s and R_L, and approximately independent of other WCS parameters. Since amplitudes of u_{rec} and i_{rec} are basically proportional to the one of u_s as mentioned above, we can say that the other parts of WCS have little effect on the rectifier circuit, and the rectifier load can be decoupled to analyze its equivalent input impedance. It is should be noticed that the rectifier circuit seems to be equivalent to a pure resistance R_L, according to (7). However, this equivalent relationship is only suitable for (7) when calculating the phase angle θ_b, and cannot be used for any other part in the rectifier load analysis.

$$\theta_b = \arctan(\omega L_s / R_L). \quad (7)$$

After getting V_d and θ_b, full response of the rectifier circuit in the positive half cycle can be calculated by (8); where, $\Phi(t)$ is the characteristic matrix of rectifier circuit; the part before the plus sign is used for solving zero-input response, and the other part is used for solving zero-state response. On the basis of (8), time domain expressions of u_{rec} and i_{rec} can be obtained, according to the symmetry of their waveforms.

$$\begin{aligned} \boldsymbol{x}(t) &= \Phi(t)\boldsymbol{x}(0) + \int_0^t \Phi(\tau)\mathbf{B}\boldsymbol{u}(t-\tau)\,d\tau \\ &= e^{\mathbf{A}t}\begin{bmatrix}0\\ V_d\end{bmatrix} + \int_0^t e^{\mathbf{A}\tau}\mathbf{B}\begin{bmatrix}V_s\sin(\omega(t-\tau)+\theta_b)\\ V_{dio}\end{bmatrix}d\tau. \end{aligned} \quad (8)$$

Finally, the fundamental wave amplitudes and phase angles of u_{rec} and i_{rec} can be calculated through Fourier transform, and defined as U_{rec_fd}, I_{rec_fd}, φ_{urec_fd}, and φ_{irec_fd}. So, the equivalent input impedance of WCS rectifier load will be given by (9); where, R_e and L_e are series equivalent resistance and inductance of the rectifier load. Only fundamental wave is considered, because the power of the harmonics is much smaller than the one of the fundamental wave. But the harmonic input impedances can also be obtained from Fourier transform. Moreover, the calculation process suggests R_e and L_e will be affected by the parameters of the rectifier circuit. Hence, the robustness of this method towards parameter variation needs to be studied. But the theoretical methods, such as calculating the derivative and root locus, cannot provide a simple and clear way to analyze the robustness in this case, since it is related to some complex or non-linear operations. So, this issue will be discussed in Section V, based on the actual parameter values.

$$\begin{aligned} R_e &= (U_{rec\_fd}/I_{rec\_fd})\cos(\varphi_{urec\_fd} - \varphi_{irec\_fd}), \\ L_e &= (U_{rec\_fd}/I_{rec\_fd})\sin(\varphi_{urec\_fd} - \varphi_{irec\_fd})/\omega. \end{aligned} \quad (9)$$

To sum up, the above analysis suggests that the rectifier load equivalent impedance contains both resistance and inductance components. Also, the series equivalent resistance and inductance can be independently calculated through parameters of rectifier circuit, and the results are basically not affected by other WCS parameters. So, the rectifier load can be decoupled with other parts of WCS, and make system design easier.

III. Compensation Network Design

Since the rectifier load has been decoupled with other parts of WCS, we are going to propose a compensation network design method, based on the rectifier load analysis and some existing researches [16-18]. Moreover, the proposed method will further decouple the primary and secondary side design, and make the WCS compensation network design simpler. As same as the rectifier load analysis, the dual-side *LCC* compensation networks are used here. The rectifier input inductance L_s should be big enough to keep the rectifier working in CCM state as mentioned above, so we will confirm it before the compensation network design. Also, the primary side compensation inductance L_p is assumed to be known, and only the four compensation capacitors are used in the design method in this section.

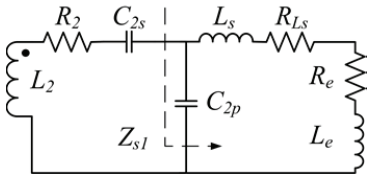

Fig. 4. Equivalent circuit of the system secondary side, considering rectifier load equivalent impedance.

Firstly, the secondary side is discussed, and its equivalent circuit is shown in Fig.4; where, the series equivalent resistance R_e and equivalent inductance L_e are used to express the rectifier load; R_2 is resistance of the receive coil. As shown in Fig.4, Z_{s1} is defined as the impedance after the secondary side series

compensation capacitor C_{2s}, and its expression is given by (10); where, $R_e'=R_e+R_{Ls}$; $L_e'=L_e+L_s$; $re(Z_{s1})$ means the real part of Z_{s1}; $im(Z_{s1})$ is the imaginary part of Z_{s1}.

$$re(Z_{s1}) = \frac{R_e' / (\omega^2 C_{2p}^{\ 2})}{R_e'^2 + (\omega L_e' - 1/(\omega C_{2p}))^2},$$
$$im(Z_{s1}) = -\frac{R_e'^2 / (\omega C_{2p}) + L_e'(\omega L_e' - 1/(\omega C_{2p}))/C_{2p}}{R_e'^2 + (\omega L_e' - 1/(\omega C_{2p}))^2}. \quad (10)$$

So, expression of the efficiency η_c can be calculated and given by (11); where, η_c is the efficiency from inverter output to rectifier load impedance; R_1 is resistance of the transmit coil; $X_{se}=im(Z_{s1})+\omega L_2-1/(\omega C_{2s})$.

$$\eta_c = \frac{re(Z_{s1})\omega^2 M^2}{(re(Z_{s1})+R_2)\omega^2 M^2 + (re(Z_{s1})+R_2)^2 R_1 + R_1 X_{se}^{\ 2}}. \quad (11)$$

Equation (11) indicates that two conditions need to be met, for the sake of achieving maximum efficiency. One is $X_{se}=0$ to minimize the denominator of η_c. The other is the load resistance of the receive coil is equal to the optimal load resistance R_{opt}, as given by (12); where, R_{opt} are obtained from the derivation of η_c, when $X_{se}=0$.

$$re(Z_{s1}) = R_{opt} = \sqrt{R_2^{\ 2} + \omega^2 M^2 R_2 / R_1}. \quad (12)$$

On the basis of (10) and (12), the secondary side parallel compensation capacitor C_{2p} can be calculated and given by (13). According to the value of C_{2p} and the equation $X_{se}=0$, the secondary side series compensation capacitor C_{2s} can also be solved. The above analysis suggests that the secondary side compensation capacitors can be designed independently of the primary side ones, and their design purpose is mainly to achieve maximum system efficiency.

$$C_{2p} = \frac{\omega L_e' + \sqrt{\omega^2 L_e'^2 - (R_e'^2 + \omega^2 L_e'^2)(1 - R_e'/R_{opt})}}{\omega (R_e'^2 + \omega^2 L_e'^2)}. \quad (13)$$

Then, the primary side is studied, and its equivalent circuit is shown in Fig.5; where, u_{inv} is inverter output equivalent voltage source; R_{Lp} is stray resistances of L_p; R_{es} is the equivalent resistance of the secondary side, when C_{2s} and C_{2p} are well designed, and $R_{es}= \omega^2 M^2/(R_{opt}+R_2)$.

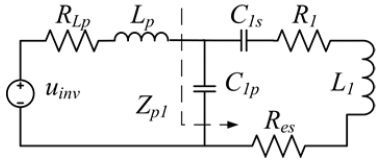

Fig. 5. Equivalent circuit of the system primary side, when the secondary side is well designed.

$$re(Z_{p1}) = \frac{(R_{es}+R_1)/(\omega^2 C_{1p}^{\ 2})}{(R_{es}+R_1)^2 + X_{pe}^{\ 2}},$$
$$im(Z_{p1}) = -\frac{(R_{es}+R_1)^2 + X_{pe}(\omega L_1 - 1/(\omega C_{1s}))}{\omega C_{1p}((R_{es}+R_1)^2 + X_{pe}^{\ 2})}. \quad (14)$$

As shown in Fig.5, Z_{p1} is defined as the impedance after the primary side compensation inductor L_p, and its expression is given by (14); where, $X_{pe}=\omega L_1-1/(\omega C_{1s})-1/(\omega C_{1p})$; $re(Z_{p1})$ means the real part of Z_{p1}; $im(Z_{p1})$ is the imaginary part of Z_{p1}.

Similar with the secondary side design, the primary side also contains two compensation capacitors with two degrees of freedom for design. So, two design targets could be added here. The first one is making the WCS output rated power. The corresponding target equation is given by (15); where, U_{inv} is the RMS value of u_{inv}; P_{or} is the rated WCS output power; η_r is the rated WCS efficiency.

$$U_{inv}^{\ 2} / re(Z_{p1}) = P_{or} / \eta_r. \quad (15)$$

The second design target is keeping the input impedance of the primary side compensation network containing a certain inductance, in order to realize the soft switching of the inverter. The corresponding target equation is given by (16); where, L_{soft} is the inductance needed for inverter soft switching.

$$im(Z_{p1})/\omega + L_p = L_{soft}. \quad (16)$$

Through simultaneously solving (15) and (16), values of the primary side compensation capacitors C_{1s} and C_{1p} can be obtained, which is not affected by the secondary side design process. Also, it should be noticed that sometimes there is no analytical solution for these equations. Numerical solution methods need to be used on this condition.

Finally, the primary and secondary side compensation networks have been decoupled for design. Also, four compensation capacitors with four degrees of freedom are designed by considering four system performance indicators, including achieving maximum efficiency, optimal load resistance, making WCS output rated power, and realizing the soft switching of the inverter. Besides, calculated values of the designed compensation capacitors require fine tuning in practice to get better results.

IV. Load Estimation Methods

The rectifier load analysis results can be used for system load estimation, which adopting the high frequency signals in WCS. The conventional load estimation methods are usually based on the pure resistance load, and also need the high frequency voltage and current at the same time [24,27]. The voltage and current sensors or probes will have different phase delays at the high frequency range, including the ones used in oscilloscopes and power analyzers. These different phase delays will lead to some deviations of the phase angle between the measured voltage and current, and affect the accuracy of the impedance calculation, especially when the phase angle is close to 90°.

In order to solve this problem, we propose a load estimation method based on the secondary side high frequency voltages. The specific process is as follows: firstly, the positive zero crossings of the rectifier input voltage (u_{rec}) and the voltage before rectifier input inductor (the voltage on C_{2p} for *LCC* topology) are detected, in order to obtain the positive zero crossing times. Then, define the positive zero crossing time of the voltage before rectifier input inductor as t_{ucs}, and the following positive zero crossing time of the rectifier input voltage as t_{urs}. So, the load estimation expression is given by (17), according to the relationship shown in (7). Finally, since

WCS has been built before load estimation, the value of the rectifier input inductor L_s can be measured, and system angle frequency ω is also known. So, the estimated load R_{L_Sesti} can be calculated through (17).

$$R_{L\_Sesti} = \omega L_s / \tan(\omega (t_{urs} - t_{ucs})). \quad (17)$$

The proposed secondary side load estimation method has considered the influence of the WCS rectifier load. Also, only high frequency voltages are used in this method; no current is adopted. Hence, it can avoid the deviations introduced by different phase delays between measured voltage and current. Besides, the proposed method only detects the positive zero crossing times, but does not need the voltage amplitudes or RMS values. This will bring some simplifications to the corresponding measurements and calculations.

However, the measured signals still need to be transmitted to the primary side by wireless communication in most cases, used for system optimization or control. In order to avoid the problems brought by wireless communication, we further put forward a load estimation method based on the primary side high frequency voltages. Here, the inverter output voltage (u_{inv}) and the voltage after inverter output inductor (the voltage on C_{1p} for *LCC* topology) are adopted. Define the fundamental voltage transfer function between the inverter output voltage and the voltage after inverter output inductor as G_p, and the fundamental voltage transfer function between the voltage before rectifier input inductor and the rectifier input voltage as G_s. The phase angle of G_s will be θ_b as defined in Fig.2, which can be adopted for load estimation based on (7). So, we need to find a relationship between G_s and G_p, and then the measured primary side voltages can be used to calculate θ_b. To achieve this, some WCS parts can be treated as a two-port network [17,18]. Hence, the coupling coils and compensation capacitors are equivalent to a two-port network as shown in Fig.6.

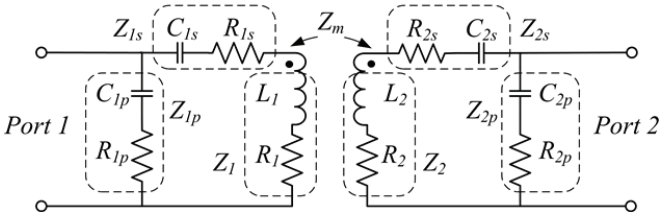

Fig. 6. Schematic of the equivalent two-port network and its parameters.

According to Fig.6, impedance parameters of the equivalent two-port network can be calculated and given by (18a).

$$\begin{aligned} Z_{11} &= Z_{1p}((Z_1 + Z_{1s})(Z_2 + Z_{2s} + Z_{2p}) - Z_m^2) / den, \\ Z_{12} &= Z_{21} = Z_{1p} Z_{2p} Z_m / den, \\ Z_{22} &= Z_{2p}((Z_2 + Z_{2s})(Z_1 + Z_{1s} + Z_{1p}) - Z_m^2) / den. \end{aligned} \quad (18a)$$

Where, Z_m=$j\omega M$, and the denominator *den* is defined by (18b).

$$den = (Z_1 + Z_{1s} + Z_{1p})(Z_2 + Z_{2s} + Z_{2p}) - Z_m^2. \quad (18b)$$

Then, the relationship between G_s and G_p can be got and given by (19a), based on the impedance parameters of the equivalent two-port network.

$$G_s = (n_1 G_p + n_2) / (d_1 G_p + d_2). \quad (19a)$$

Where, the coefficients n_1, n_2, d_1, and d_2 are defined by (19b); where, Z_p=R_{Lp}+$j\omega L_p$; Z_s=R_{Ls}+$j\omega L_s$.

$$\begin{aligned} &n_1 = Z_{12}Z_{21} - Z_{11}Z_{22},\ d_2 = (Z_{11} + Z_p)(Z_{22} + Z_s) - Z_{12}Z_{21}, \\ &n_2 = Z_p Z_{22} + Z_{11}Z_{22} - Z_{12}Z_{21},\ d_1 = Z_{12}Z_{21} - Z_{11}(Z_{22} + Z_s). \end{aligned} \quad (19b)$$

Furthermore, the amplitudes and phase angles of the selected voltages will be measured in the primary side, and then the transfer function G_p can be obtained. Define the amplitude of G_p as *Amp*, and the phase angle of G_p as *Php*. So, θ_n, which is the phase angle of the numerator of G_s, can be calculated, as well as θ_d, which is the phase angle of the denominator of G_s. Their expressions are given by (20).

$$\begin{aligned} \theta_n &= \arctan \frac{Amp \cdot amn1 \cdot \sin(Php + phn1) + imn2}{Amp \cdot amn1 \cdot \cos(Php + phn1) + ren2}, \\ \theta_d &= \arctan \frac{Amp \cdot amd1 \cdot \sin(Php + phd1) + imd2}{Amp \cdot amd1 \cdot \cos(Php + phd1) + red2}. \end{aligned} \quad (20)$$

Where, *amn*1 and *phn*1 are the amplitude and phase angle of n_1; *amd*1 and *phd*1 are the amplitude and phase angle of d_1; *ren*2 and *imn*2 are the real and imaginary parts of n_2; *red*2 and *imd*2 are the real and imaginary parts of d_2; they can be calculated through (18) and (19), according to the measured values of the WCS parameters.

Finally, we can get the phase angle of G_s, and the estimated load R_{L_Pesti} can be calculated through (21). Moreover, the derivation process suggests that R_{L_Pesti} will be affected by WCS parameters, such as mutual-inductance *M*, compensation capacitances C_{1s}, C_{1p}, C_{2s}, C_{2p}, and so on. Hence, the robustness of the estimation methods needs to be studied, when these parameters vary. But similar with the case of the rectifier equivalent load calculation method in Section II, the theoretical methods cannot provide a simple and clear way to analyze the robustness. So, this issue will be also discussed in Section V, based on the actual parameter values.

$$R_{L\_Pesti} = \omega L_s / \tan(\theta_n - \theta_d). \quad (21)$$

Developed from the above secondary side load estimation method, the proposed primary side load estimation method has also considered the influence of the rectifier load. Meanwhile, it only adopts high frequency voltages, and can avoid the phase delay deviations, too. The difference is this method needs to measure voltage amplitudes. But on the other side, it does not require wireless communication between the primary and secondary sides. So, it has some advantages in EV applications.

V. Experimental Verification And Analysis

A. Experiment Layout and System Parameters

An EV wireless charging prototype is developed to verify the rectifier load analysis results and the proposed methods. Its configuration is shown in the photograph in Fig.7. A full-bridge single-phase inverter with MOSFETs is assigned as the power source. System load is a full-bridge diode rectifier with load resistors. The transmit coil is rounded rectangular with spiral disc type of fifteen turns of Litz wires. The receive coil is square with spiral disc type of twenty turns of Litz wires. The Litz wire used for coils is 640 strands with 0.1 mm diameter for

This article has been accepted for publication in a future issue of this journal, but has not been fully edited. Content may change prior to final publication. Citation information: DOI 10.1109/TIE.2018.2793260, IEEE Transactions on Industrial Electronics

each strand. Also, ferrites are adopted as the core material of the coils, and aluminum plates are added outside the ferrites for more shielding. The transmit coil size is 58 cm × 42 cm, and the receive coil size is 32 cm × 32 cm. The vertical distance between the coils is 20 cm.

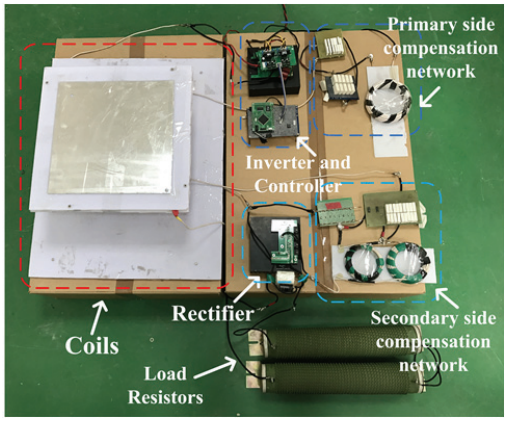

Fig. 7. Photograph of the developed EV wireless charging prototype.

The prototype is designed with rated output power 3.3 kW on the input DC voltage 400 V. System operation frequency is 85 kHz. Load resistance R_L is 42.9 Ω, which is selected according to an EV power battery with about 325 V - 340 V open-circuit voltage and 8 A charging current. System impedance parameter values are measured by a LCR meter, and the results are given as follows. Self-inductances values of the transmit coil and receive coil are 232.9 uH and 219.7 uH. Mutual-inductance value is 25.4 uH, when the receive coil is aligned with the transmit coil. Compensation inductors L_p and L_s are selected to be 79.9 uH and 83.3 uH. Based on the design method in Section III, the compensation capacitors can be obtained as follows: C_{1s}=19.7 nF, C_{1p}=82.8 nF, C_{2s}=23.6 nF, C_{2p}=69.6 nF. The above parameter values are defined as the standard parameter values, which can make the system achieve good performances, such as rated output power, high efficiency, inverter soft switching, etc. In the following sections, some of these parameters will be changed to different values for further verifications and discussions.

The type of MOSFET is IPW65R037C6. Also, the values of V_{dio} and R_{dio} will vary with the junction temperature T_j (in degrees Celsius), as shown in the datasheet of the diode C3D16060D, which is used in the developed prototype. So, their values can be obtained from the measured temperature by a thermal imager and the following equations in the datasheet: $V_{dio} = 0.93+((-9.3\times10^{-4})\times T_j)$; $R_{dio} = 0.058+((5.7\times10^{-4})\times T_j)$.

B. Rectifier Equivalent Load Verifications and Analysis

Based on the developed EV wireless charging prototype, the calculation method of the rectifier load equivalent impedance is verified, and the equivalent load characteristics are studied. Firstly, experimental waveforms of the rectifier input voltage and current are given in Fig. 8(a), under the condition of standard parameter values. It shows that the waveform of rectifier input current has some distortion, which is the same as shown in Fig.2. Moreover, import the experimental data to the software Matlab, and the amplitudes and phase angles of the fundamental waves will be calculated through the FFT (fast Fourier transform) program. So, the fundamental waves can be drawn by Matlab and shown in Fig. 8(b). It suggests that the fundamental wave of rectifier input current lags behind the one of rectifier input voltage, which means the rectifier input impedance contains a certain inductance component. This conclusion is consistent with the one obtained in Section II.

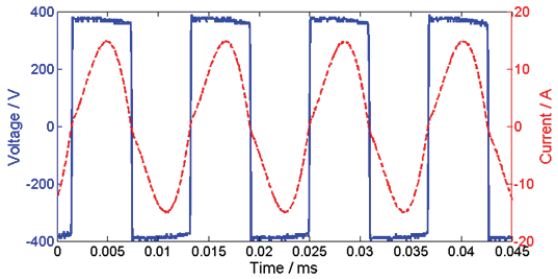

(a) Rectifier input voltage and current waveforms.

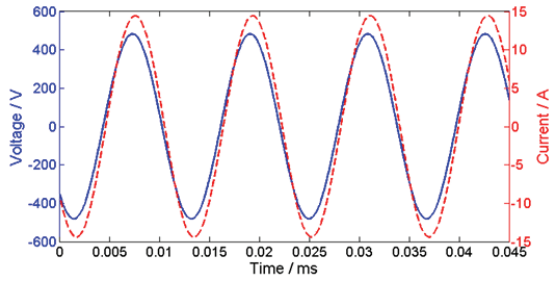

(b) Calculated fundamental waves.

Fig. 8. Experimental results of rectifier input voltage and current, as well as their fundamental waves, based on the standard parameter values.

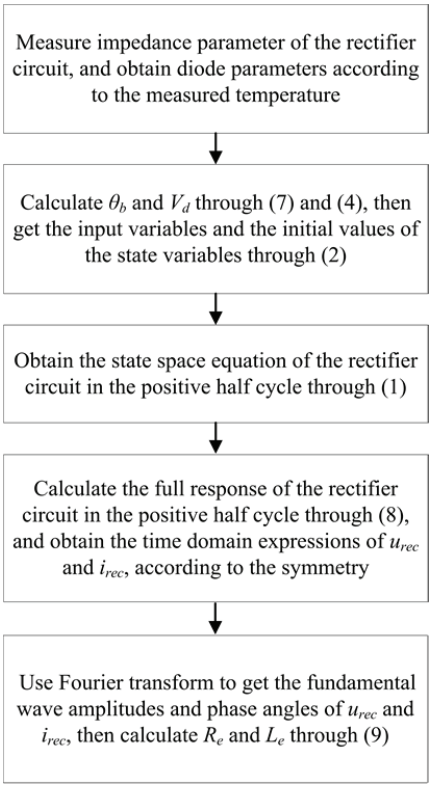

Fig. 9. Flow chart of the proposed method used to calculate the rectifier equivalent load.

This article has been accepted for publication in a future issue of this journal, but has not been fully edited. Content may change prior to final publication. Citation information: DOI 10.1109/TIE.2018.2793260, IEEE Transactions on Industrial Electronics

Then, the rectifier equivalent load calculation method is verified on conditions of different load resistances and rectifier input inductances. Based on the analysis in Section II, the equivalent resistance and inductance can be calculated through the process in the flow chart in Fig.9.

Following the steps in Fig.9, the equivalent impedances of the rectifier load can be calculated and given in Tab.1. Also, the experimental ones are shown in Tab.1, which are obtained from the fundamental amplitude and phase angle calculation results of the experimental waveforms.

TABLE I
COMPARISONS BETWEEN CALCULATED AND EXPERIMENTAL RECTIFIER EQUIVALENT LOADS BASED ON DIFFERENT PARAMETER VALUES

Prototype Parameter Values		Calculated Equivalent Load		Experimental Equivalent Load	
R_L (Ω)	L_s (uH)	R_e (Ω)	L_e (uH)	R_e (Ω)	L_e (uH)
42.9	83.3	33.1	10.5	33.0	10.2
	113.9	33.8	7.7	33.7	8.2
	49.1	30.4	16.9	32.7	18.2
21.5	83.3	17.1	2.1	17.4	2.5
	113.9	17.3	1.4	17.2	1.7
	49.1	16.6	3.9	17.5	4.6

Tab.1 suggests that the equivalent resistance and inductance will both reduce when R_L becomes smaller. While, the equivalent resistance is not affected much by L_s, and the equivalent inductance will increase when L_s becomes smaller. Further calculations indicate that on the condition of standard parameter values, the difference between the calculated and experimental equivalent resistances is only 0.1 Ω, and the calculation error of the equivalent inductance is smaller than 3%. This means the proposed method has good accuracy, when the system is well designed and working in the rated state. However, when L_s is changed to 49.1 uH, the calculation error has increased to 7%. This is caused by the value of L_s is too small to make the rectifier working in the discontinuous conduction mode (DCM). Also, when R_L is changed to 21.5 Ω, the relative error percentages increase, due to the small values of equivalent inductances. But the absolute errors are still small. So, the calculated results are basically close to the experimental ones, which have proved the effectiveness of the rectifier load model and the equivalent impedance calculation method.

However, there is a trend that L_e becomes smaller when R_L decreases. So, if R_L has a small value about a few ohms, L_e will be very small. When the power battery voltage remains the same while the charging current has increased to 80 A or higher, the equivalent system load resistance will be a few ohms. This case may happen when WCS is used for the fast charging of the passenger cars, or the normal charging for the heavy duty vehicles. The output power of this kind of WCS is usually more than 20 kW, even reaches more than 100 kW. Under these conditions, L_e is much smaller than the rectifier input inductance L_s, and its effect is ignorable. But the slow charging for the passenger cars (with output power lower than 10 kW) still hold a considerable proportion, so the proposed rectifier equivalent load calculation method could also be useful for the analysis and design of EV wireless charging system.

Moreover, the calculated and experimental values of the equivalent resistances are close to the ones got by conventional method (34.77 Ω and 17.43 Ω), which adopts the coefficient $8/\pi^2$ as the relationship between the rectifier input impedance and the system load resistance [5,6]. This indicates the conventional method can be approximately used for equivalent resistance calculation. However, it ignores the equivalent inductance, as well as the effects of rectifier circuit parameters.

Furthermore, the influences of other WCS parameters on the rectifier equivalent load are investigated. When DC source voltage is changed to 200 V and other parameters still have standard values, the calculated equivalent load is 33.1 Ω and 10.5 uH; while, the experimental one is 33.1 Ω and 10.6 uH. When the receive coil has a lateral misalignment distance of 10 cm, and other parameters still have standard values, the calculated equivalent load is 33.1 Ω and 10.5 uH; while, the experimental one is 32.9 Ω and 10.3 uH. These results suggest other WCS parameters, such as DC source voltage and mutual-inductance, basically have no effect on the rectifier equivalent load. So, the rectifier load can be modeled and analyzed, decoupling with other parts of WCS.

Finally, the robustness of the proposed rectifier equivalent load calculation method is discussed towards parameter uncertainties. The parameter uncertainties are mainly caused by the measurement errors and the stray parameters. Also, the diode parameter values V_{dio} and R_{dio} will change with the junction temperature T_j. Since the junction temperature of the diode cannot be measured directly, and only can be estimated by the device surface temperature, so this will lead to parameter uncertainties of the rectifier, too. The nominal accuracy of the LCR meter used for measurements is 0.05%. Hence, the influence of the measurement error will be very small, and the impact of T_j is adopted here to analyze the robustness.

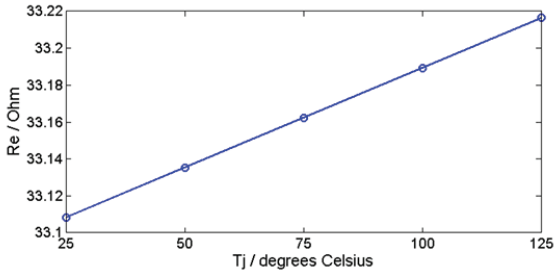

(a) Calculation results of the equivalent resistance R_e.

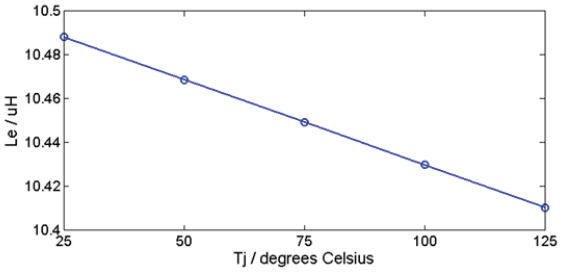

(b) Calculation results of the equivalent inductance L_e.

Fig. 10. Rectifier equivalent load calculation results, when the diode parameter values V_{dio} and R_{dio} change with the junction temperature T_j.

The junction temperature T_j is usually 25-125 degrees

This article has been accepted for publication in a future issue of this journal, but has not been fully edited. Content may change prior to final publication. Citation information: DOI 10.1109/TIE.2018.2793260, IEEE Transactions on Industrial Electronics

Celsius in the WCS normal working conditions. So, the rectifier equivalent load calculation results are shown in Fig.10, when the diode parameter values V_{dio} and R_{dio} change with the junction temperature T_j. Fig.10 suggests that the change of the junction temperature only has a small impact on the rectifier equivalent load calculation results. Also, the previous analysis shows that the calculation method can achieve high accuracy, on conditions of different system load resistances, rectifier input inductances, DC voltages, and mutual-inductances. So, the proposed rectifier equivalent load calculation method has good robustness, in the cases of WCS parameter variations. Besides, it should be noticed that in the practice case, the equivalent resistance of the power battery will change in the charging process, and this will bring the variation of the rectifier input impedance. Further work may be focused on the dynamic process and features of both the WCS and the rectifier load during charging.

C. Effects of Rectifier Load Equivalent Inductance

Since the conventional design methods usually neglect the equivalent inductance of the rectifier load [19-21], we are going to discuss its effects. Fig.11 shows the simulation results of L_e effects, which are conducted by Matlab, according to the actual parameter values of the developed EV wireless charging prototype. These simulations have not considered the switching losses of power converters, and other stray losses. So, the values of the simulated output powers and efficiencies will be a little larger than the experimental ones.

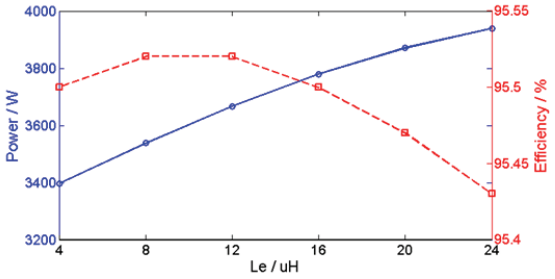

Fig. 11. Simulation results of L_e effects on output power and efficiency.

Fig.11 suggests the influence of L_e on efficiency is very small. However, the output power changes from about 3.4 kW to more than 3.9 kW, when L_e varies. Considering the rated system output power 3.3 kW, the change range is more than 15%, under the influence of the equivalent inductance. Hence, L_e will significantly affect the output power, and the system output power will have obvious deviation with the rated one, if the compensation networks are designed without considering its influence.

In order to further prove this conclusion, we have designed another group of compensation capacitors, based on the conventional $8/\pi^2$ rectifier load calculation method and ignoring L_e. Because the primary and secondary side compensation network designs are decoupled, and L_e only affects the design results in the secondary side as mentioned in Section III, the secondary side compensation capacitors have been redesigned as follows: C_{2s}=22.4 nF, C_{2p}=73.3 nF; while the primary side compensation capacitors remain the same. Since the original compensation capacitors are designed through the method proposed in Section III, they aim to achieve the maximum efficiency and the rated output power at the same time, which is 3.3 kW for the developed EV wireless prototype.

The experimental results have shown that system efficiency can reach as high as 93.5%, and output power is 3.33 kW, which is very close to the design target of the rated output power 3.3 kW, on the condition of adopting the original compensation capacitor values. However, when ignoring L_e to design the compensation capacitors, the experimental results show that the measured system efficiency is 93.2%; while the measured output power has increased to 3.95 kW, which is more than 600 W higher than the design target of the rated output power. In this case, the reactive power in WCS will increase, and bring large electric stresses to the system devices, even affect the safe operation of WCS. Hence, these experiments have shown that the equivalent inductance of the rectifier load should be considered for system design and analysis. Also, they have proved the effectiveness of the proposed compensation network design method, which can make WCS achieve high efficiency and rated output power.

D. Verifications of Load Estimation Methods

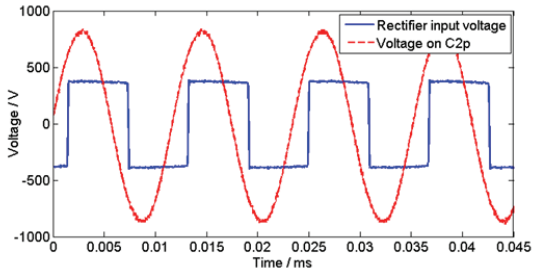

(a) Measured voltages used for secondary side load estimation.

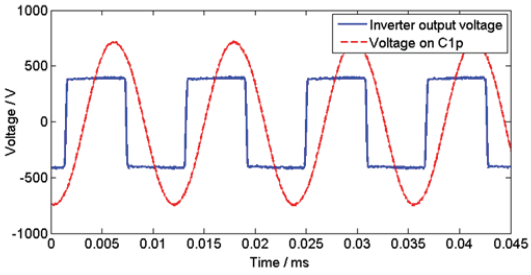

(b) Measured voltages used for primary side load estimation.

Fig. 12. Experimental results of the system voltages used for load estimations based on the standard parameter values.

Based on the developed EV wireless charging prototype, the proposed secondary and primary side load estimation methods can be verified. Fig.12 shows the measured system voltages used for load estimations, under the condition of standard parameter values; where, measured voltages in Fig. 12(a) are used for secondary side load estimation, and the ones in Fig. 12(b) are used for primary side load estimation. Through these experimental results, the positive zero crossing times can be directly extracted from the measured data, when the measured voltage value turns from negative to positive. Also, the fundamental amplitudes of the measured voltages can be calculated by the FFT program in Matlab, to get the amplitude of the fundamental voltage transfer function G_p. So according

This article has been accepted for publication in a future issue of this journal, but has not been fully edited. Content may change prior to final publication. Citation information: DOI 10.1109/TIE.2018.2793260, IEEE Transactions on Industrial Electronics

to the measured voltages, the amplitude and phase angle of G_p can be obtained, and the system load resistance can be estimated through the process in the flow chart in Fig.13.

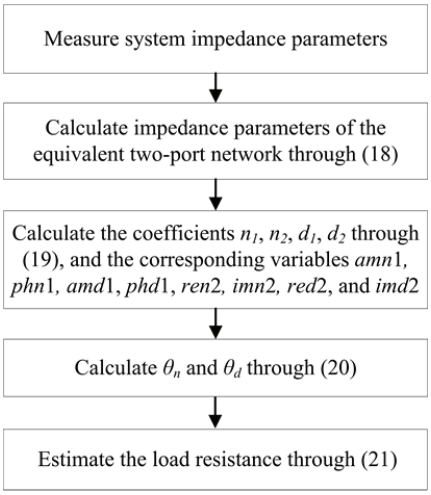

Fig. 13. Flow chart of the proposed load estimation method based on the measured primary side voltages.

TABLE II
LOAD ESTIMATION RESULTS USING PROPOSED SECONDARY AND PRIMARY SIDE LOAD ESTIMATION METHODS

Prototype Parameter Values		Secondary Side Load Estimation Method	Primary Side Load Estimation Method
R_L (Ω)	L_s (uH)	R_{L_Sesti} (Ω)	R_{L_Pesti} (Ω)
42.9	83.3	41.3	43.5
	113.9	41.5	44.9
	49.1	39.4	44.6
21.5	83.3	21.2	24.4
	113.9	21.3	24.7
	49.1	20.7	24.1

Following the steps in Fig.13, the load estimation results can be obtained and given in Tab.2, on conditions of different load resistances and rectifier input inductances. Tab.2 suggests that for the secondary side load estimation method, the estimation error is 3.7% on the condition of standard parameter values. This means the proposed method has good accuracy, when the system is well designed and working in the rated state. But when L_s is changed to 49.1 uH, the estimation error has increased to 8.2%, due to the DCM working state of the rectifier. Also, when R_L is changed to 21.5 Ω, the maximum estimation error is only 3.7%. The estimation errors are mainly caused by the measurement deviations of the voltage zero crossing times, and the influences of the filter capacitor and its stray resistance, which have been neglected in the initial value calculation process of the rectifier circuit. Moreover, for the primary side load estimation method, Tab.2 suggests its estimation error is 1.4% on the condition of standard parameter values, which means it also performs well. However, the estimation errors obviously increase, on the conditions that R_L is equal to 21.5 Ω. This can be explained by the primary side load estimation method needs the measured parameter values of WCS, which all have certain measurement deviations. When R_L has changed to 21.5 Ω, the phase angles of the voltage transfer functions become bigger and closer to 90°, so the measurement deviations will be more easily amplified by the tangent function in (21).

Moreover, the robustness of the proposed primary side load estimation method is discussed towards parameter uncertainties. The impact of the stray parameter is adopted to analyze the robustness here. The major stray parameter in WCS is the inductance of the connecting cables, which is not included in the established system model. These cables are usually used to connect coils to other parts, or be the lead wires of the inductors. So, they mainly affect values of the coils and compensation inductances. According to measurements of these cables, their stray inductances are smaller than or about 1 uH. In order to make its influences more obvious, we select this value as ±1.5 uH. Since the stray inductances are too small to be conducted in experiments, simulations are adopted here. Taking the conditions that L_1 has the inductance with ±1.5uH errors as an example, the simulation results are shown Fig.14. Further calculation based on Fig.14 indicates that the estimation error reaches to almost 6%, when L_1 has the inductance with 1.5 uH error. This error is obvious and the stray inductance should be considered when estimating the system load. So, the connecting cables of the coils and the lead wires of the inductors are taken into count, when we measured the parameter values. Since the effects of the major stray parameter in WCS are considered, the proposed load estimation methods have good robustness, on conditions that stray parameters exist.

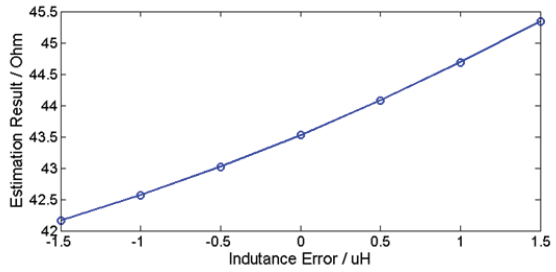

Fig. 14. Simulated load estimation results of the proposed primary side method, when L_1 has the inductance with ±1.5uH errors.

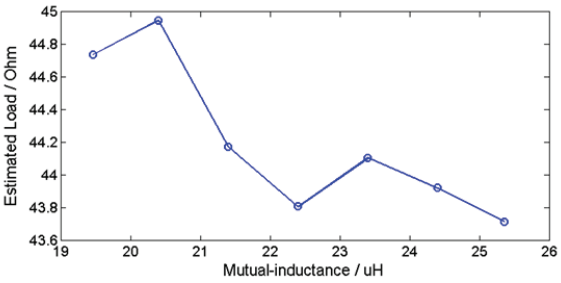

Fig. 15. Simulated load estimation results of the proposed primary side method, when M varies about 23%.

Furthermore, the robustness of the proposed primary side load estimation method is proved, when the mutual-inductance M is changeable. Through measurement and calculation, M is 19.5 uH with 15 cm lateral misalignment. In this case, M variation is more than 23%, when the lateral misalignment distance changes from 0 cm to 15 cm. Based on the actual parameter values, simulated load estimation results are shown in Fig.15. Further calculation indicates that the maximum

estimation error is smaller than 3%, when M varies about 23%. Then, the experiments show that when the receive coil has a lateral misalignment distance of 10 cm, and other parameters still have standard values, R_{L_Sesti} is 41.7 Ω, and R_{L_Pesti} is 44.7 Ω; while the estimation errors are 2.8% and 4.2%, respectively. These experimental errors are also small. So, the proposed load estimation methods have good robustness, on conditions of mutual-inductance M variation.

Finally, the robustness of the proposed primary side load estimation method is analyzed, when the compensation capacitances C_{1s}, C_{1p}, C_{2s}, and C_{2p} have 25% variations. Based on the actual parameter values, simulated estimation error percentages are shown in Fig.16, compared with the system load resistance 42.9 Ω. In Fig.16, the cases of compensation capacitances increasing by 25% are taken as examples. It is clear that the estimation errors are almost in the range of ±3%, when the compensation capacitances vary 25%. Then, the experimental results are given, considering the related analysis in Section V. C. When the secondary side compensation capacitances have been changed to 22.4 nF and 73.3 nF, and other WCS parameters still have standard values, R_{L_Sesti} will be 40.9 Ω, and R_{L_Pesti} will be 44.2 Ω; while the estimation errors are 4.7% and 3.0%, respectively. These experimental results have shown that the maximum estimation error is less than 5%. So, the proposed load estimation methods have good robustness, on conditions of compensation capacitance variations.

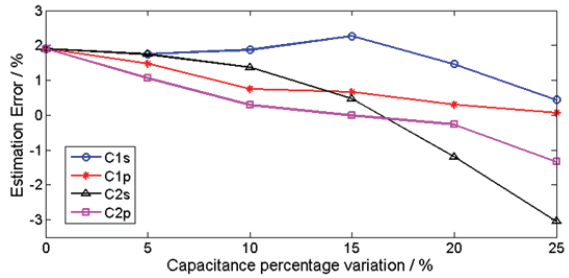

Fig. 16. Simulated load estimation errors of the proposed primary side method, when the compensation capacitances vary 25%.

Besides, when DC source voltage is changed to 200 V and other parameters still have standard values, R_{L_Sesti} is 41.7 Ω, and R_{L_Pesti} is 43.8 Ω; while the estimation errors are 2.8% and 2.1%, respectively. So, these experimental results have shown that the proposed load estimation methods have good robustness, on conditions of DC source voltage variation.

To sum up, although there are some deviations, the estimated load resistances are basically close to the actual values of the system load resistors. This has proved the effectiveness and robustness of the proposed secondary and primary side load estimation methods. Further work may be focused on reducing the measurement deviation effects of both the voltages and the WCS parameters, in order to improve the accuracy of the load estimation methods, especially on conditions that phase angles of the voltage transfer functions are close to 90°.

VI. Conclusion

This paper presents a systematic analysis of the rectifier load used for EV wireless charging system. The rectifier load model has been established to calculate its equivalent input impedance, which contains both resistance and inductance components, and can be independently calculated through the parameters of the rectifier circuit. Based on the rectifier load analysis, a compensation network design method is proposed to achieve the decoupling design of the primary and secondary side compensation capacitors. Furthermore, a secondary side load estimation method and a primary side load estimation method are put forward, considering the influence of the rectifier load. They adopt only measured voltages to avoid the deviations introduced by different phase delays between measured voltage and current. Finally, the established model, the proposed rectifier load calculation method, compensation network design method, secondary and primary side load estimation methods have been verified, based on the developed EV wireless charging prototype. The experimental results have shown the following conclusions: the equivalent input impedance of rectifier load is mainly affected by system load resistance and rectifier input inductance; rectifier load equivalent inductance will impact system performances, and should be considered for compensation network design; the proposed load estimation methods have good accuracy, but still need to be improved in further research; the proposed rectifier load calculation method and system load estimation methods all have good robustness, on conditions of WCS parameter variations.

Although the works in this paper are conducted based on the specific system, they can be extended to more applications, such as wireless charging systems with other rectifier or compensation network topologies, etc. They will be helpful for system design and control to make EV wireless charging systems achieve stable operation and high performance.

References

[1] S. Q. Li, and C. C. Mi, "Wireless power transfer for electric vehicle applications," *IEEE J. Emerg. Sel. Topics Power Electron.*, vol. 3, no. 1, pp. 4-17, Mar. 2015.

[2] Y. D. Ko, and Y. J. Jang, "The optimal system design of the online electric vehicle utilizing wireless power transmission technology," *IEEE Trans. Intell. Transp. Syst.,* vol. 14, no. 3, pp. 1255-1265, Sep. 2013.

[3] W. X. Zhong, and S. Y. R. Hui, "Maximum energy efficiency tracking for wireless power transfer systems," *IEEE Trans. Power Electron.,* vol. 30, no. 7, pp. 4025-4034, Jul. 2015.

[4] D. Ahn, S. Kim, J. Moon, and I. K. Cho, "Wireless power transfer with automatic feedback control of load resistance transformation," *IEEE Trans. Power Electron.,* vol. 31, no. 11, pp. 7876-7886, Nov. 2016.

[5] M. P. Theodoridis, "Effective capacitive power transfer," *IEEE Trans. Power Electron.,* vol. 27, no. 12, pp. 4906-4913, Dec. 2012.

[6] D. Thenathayalan, and J. H. Park, "Wide-air-gap transformer model for the design-oriented analysis of contactless power converters," *IEEE Trans. Ind. Electron.,* vol. 62, no. 10, pp. 6345-6359, Oct. 2015.

[7] M. Fu, Z. Tang, M. Liu, C. Ma, and X. Zhu, "Full-bridge rectifier input reactance compensation in megahertz wireless power transfer systems," in *Proc. 2015 WoW,* 2015, pp. 1-5.

[8] A. Berger, M. Agostinelli, S. Vesti, J. A. Oliver, J. A. Cobos, and M. Huemer, "A wireless charging system applying phase-shift and amplitude control to maximize efficiency and extractable power," *IEEE Trans. Power Electron.,* vol. 30, no. 11, pp. 6338-6348, Nov. 2015.

[9] K. Colak, E. Asa, M. Bojarski, D. Czarkowski, and O. C. Onar, "A novel phase-shift control of semibridgeless active rectifier for wireless power transfer," *IEEE Trans. Power Electron.,* vol. 30, no. 11, pp. 6288-6297, Nov. 2015.

[10] Y. Akihara, T. Hirose, S. Masuda, N. Kuroki, M. Numa, and M. Hashimoto, "Analytical study of rectifier circuit for wireless power transfer systems," in *Proc. ISAP,* 2016, pp. 338-339.

[11] H. C. Li, K. P. Wang, L. Huang, W. J. Chen, and X. Yang, "Dynamic modeling based on coupled modes for wireless power transfer systems," *IEEE Trans. Power Electron.,* vol. 30, no. 11, pp. 6245-6253, Nov. 2015.

[12] S. Aldhaher, P. C. K. Luk, K. E. K. Drissi, and J. F. Whidborne, "High-input-voltage high-frequency class E rectifiers for resonant inductive links," *IEEE Trans. Power Electron.,* vol. 30, no. 3, pp. 1328-1335, Mar. 2015.

[13] H. T. Shi, J. D. Mao, X. S. Li, and J. T. Pan, "Modeling and analysis of impedance for uncontrolled rectifier based nonlinear load," in *Proc. CCDC,* 2016, pp. 1770-1775.

[14] C. K. Lee, S. Kiratipongvoot, and S. C. Tan, "High-frequency-fed unity power-factor AC-DC power converter with one switching per cycle," *IEEE Trans. Power Electron.,* vol. 30, no. 4, pp. 2148-2156, Apr. 2015.

[15] Q. Lei, M. Shen, V. Blasko, and F. Z. Peng, "A generalized input impedance model of three phase diode rectifier," in *Proc. APEC,* 2013, pp. 2655-2661.

[16] S. Q. Li, W. H. Li, J. J. Deng, T. D. Nguyen, and C. C. Mi, "A double-sided LCC compensation network and its tuning method for wireless power transfer," *IEEE Trans. Veh. Technol.*, vol. 64, no. 6, pp. 2261-2273, Jun. 2015.

[17] M. Dionigi, M. Mongiardo, and R. Perfetti, "Rigorous network and full-wave electromagnetic modeling of wireless power transfer links," *IEEE Trans. Microwave Theory Tech.*, vol. 63, no. 1, pp. 65-75, Jan. 2015.

[18] A. Costanzo, M. Dionigi, F. Mastri, M. Mongiardo, G. Monti, J. A. Russer, P. Russer, and L. Tarricone, "Conditions for a load-independent operating regime in resonant inductive WPT," *IEEE Trans. Microwave Theory Tech.*, vol. 65, no. 4, pp. 1066-1076, Apr. 2017.

[19] Q. W. Zhu, L. F. Wang, and C. L. Liao, "Compensate capacitor optimization for kilowatt-level magnetically resonant wireless charging system," *IEEE Trans. Ind. Electron.,* vol. 61, no. 12, pp. 6758-6768, Dec. 2014.

[20] J. W. Kim, D. H. Kim, and Y. J. Park, "Analysis of capacitive impedance matching networks for simultaneous wireless power transfer to multiple devices," *IEEE Trans. Ind. Electron.,* vol. 62, no. 5, pp. 2807-2813, May 2015.

[21] J. Kim, and J. Jeong, "Range-adaptive wireless power transfer using multiloop and tunable matching techniques," *IEEE Trans. Ind. Electron.,* vol. 62, no. 10, pp. 6233-6241, Oct. 2015.

[22] W. H. Li, H. Zhao, S. Q. Li, J. J. Deng, T. Z. Kan, and C. C. Mi, "Integrated LCC compensation topology for wireless charger in electric and plug-in electric vehicles," *IEEE Trans. Ind. Electron.,* vol. 62, no. 7, pp. 4215-4225, Jul. 2015.

[23] J. P. W. Chow, H. S. H. Chung, and C. S. Cheng, "Use of transmitter-side electrical information to estimate mutual inductance and regulate receiver-side power in wireless inductive link," *IEEE Trans. Power Electron.,* vol. 31, no. 9, pp. 6079-6091, Sep. 2016.

[24] J. Yin, D. Lin, C. K. Lee, and S. Y. R. Hui, "A systematic approach for load monitoring and power control in wireless power transfer systems without any direct output measurement," *IEEE Trans. Power Electron.,* vol. 30, no. 3, pp. 1657-1667, Mar. 2015.

[25] Z. H. Wang, Y. P. Li, Y. Sun, C. S. Tang, and X. Lv, "Load detection model of voltage-fed inductive power transfer system," *IEEE Trans. Power Electron.,* vol. 28, no. 11, pp. 5233-5243, Nov. 2013.

[26] M. F. Fu, H. Yin, X. Zhu, and C. B. Ma, "Analysis and tracking of optimal load in wireless power transfer systems," *IEEE Trans. Power Electron.,* vol. 30, no. 7, pp. 3952-3963, Jul. 2015.

[27] J. Yin, D. Lin, T. Parisini, and S. Y. R. Hui, "Front-end monitoring of the mutual inductance and load resistance in a series-series compensated wireless power transfer system," *IEEE Trans. Power Electron.,* vol. 31, no. 10, pp. 7339-7352, Oct. 2016.

[28] M. Feliziani, T. Campi, S. Cruciani, F. Maradei, U. Grasselli, M. Macellari, and L. Schirone, "Robust LCC compensation in wireless power transfer with variable coupling factor due to coil misalignment," in *Proc. 2015 EEEIC,* 2015, pp. 1181-1186.

[29] M. Liu, Y. Qiao, and C. B. Ma, "Robust optimization for a 6.78-MHz wireless power transfer system with class E rectifier," in *Proc. 2016 WoW,* 2016, pp. 88-94.

[30] H. Feng, T. Cai, S. X. Duan, J. B. Zhao, X. M. Zhang, and C. S. Chen, "An LCC-compensated resonant converter optimized for robust reaction to large coupling variation in dynamic wireless power transfer," *IEEE Trans. Ind. Electron.,* vol. 63, no. 10, pp. 6591-6601, Oct. 2016.

Yanjie Guo received the Ph.D degree in 2013 from the Institute of Electrical Engineering, Chinese Academy of Sciences (IEECAS).

Now he is an associate professor at the Department of Vehicle Energy System and Control Technology, IEECAS, and also at the Key Laboratory of Power Electronics and Electric Drive, Chinese Academy of Sciences. His research interests include wireless power transfer modeling and design, stationary wireless EV charging system, dynamic wireless EV charging system, electromagnetic compatibility (EMC), power electronics applications, and electromagnetic field analysis.

Lifang Wang (M'09) got her Ph.D degree in 1997 from Jilin University. After that she joined the Institute of Electrical Engineering, Chinese Academy of Sciences (IEECAS). During the Chinese tenth-five year plan (2001-2005), she was a member of the national specialist group of Key Special Electric Vehicle Project of the National 863 Program, and she was the head of the 863 Special EV Project Office.

She is currently the director of Department of Vehicle Energy System and Control Technology at IEECAS. She is also the vice director of Key Laboratory of Power Electronics and Electric Drive, Chinese Academy of Sciences. Her research interests include wireless charging system for EV, electric vehicle control system, EV battery management system, electromagnetic compatibility, and smart electricity use. She has directed more than 15 projects in these fields and has published more than 90 papers and 30 patents.

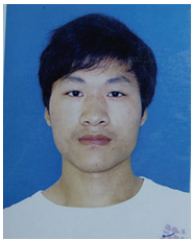

Yuwang Zhang received the M.S. degree in electronic science and technology from the Wuhan University of Technology in 2015. He is currently working toward the Ph.D. degree at the Institute of Electrical Engineering, Chinese Academy of Sciences (IEECAS).

His research interests include wireless power transfer theory, optimization and control of electric vehicle wireless charging system, bi-directional wireless charging system.

Shufan Li received his M.S. degree in electrical engineering from the University of Chinese Academy of Sciences in 2016. He is currently working toward the Ph.D. degree at the Institute of Electrical Engineering, Chinese Academy of Sciences (IEECAS).

His research interests include wireless power transfer theory, parameter estimation and control of wireless charging system, dynamic wireless EV charging system.

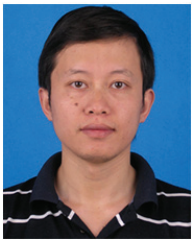

Chenglin Liao (M'09) received the Ph.D. degree in Power Machinery and Engineering from Beijing Institute of Technology, Beijing, China, in 2001. After that he had spent 2 years as a postdoctoral researcher at the Tsinghua University.

He is now the deputy director of Department of Vehicle Energy System and Control Technology, Institute of Electrical Engineering, Chinese Academy of Sciences (IEECAS). His currently research is mainly on the development of wireless charging system for electric vehicles.